Version: March 15, 1996

The Spatial Intensity Distribution of the UV light in HH objects. Revisited.

Amaya Moro-Martin

Maria Mite.hell Observatory, Nantucket, MA 02554

email: mamoro@mmo.org

Alberto Noriega-Crespo

Infrared Processing and Analysis Center, Calrl'cell-Jl'l,, Pasadena, CA 91125

and Maria, Mitchell Observatory, Nantucket, M A 02554

email: alberto@ipac.caltech.edu

Karl-Heinz Böhm

Department of Astronomy FM-20, University of Washington, Seattle, WA 98195

email: bohm@astro.washington.edu

and

Alejandro C. Raga

Instituto de Astronomía, UNAM, 04510, México D.F., México

email: raga@astroscu.unam.mx

RESUMEN

Muchas de las características observadas en objetos Herbig-Haro han podido ser reproducidas mediante modelos de choque. Se muestra que modelos similares pueden aplicarse para la distribución espacial de intensidad de las lineas ultravioleta observadas por IUE. Se han utilizado espectros del archivo de IUE para estudiar las lineas ultraviolet (C IV λ1549,

Si III] λ1891, C 111] λ1909, C II] λ2326, Mg 11 λ2799) y también el continuo (modelado como continuo de dos fotones), de Ios objetos: 11111, 1111 2(11 -I A'), 1111 2(G-111)) IIII 24A, IIII 32A, 1111 43(A-I 11-I C) y IIII 47A. Los dates de IUE tienen un calidad limitada, debido a lo amplio de su función de ensanchamiento de punto y su baja señal a ruido, y por tanto han s i d o degradados para com pararlos con l as obser vaci ones. l,Os parámetros físicos de los models sc basan en estudios ópticos anteriores y fueron variados dentro de sus

ABSTRACT

Simple kinematical bow shock models have successfully explained many of the observed features in Ilcrbig-11 aro objects. It is shown that similar models can be applied to the spatial intensity distribution of the UV lines observed by IUE. Archival IUE spectra have been used for the objects 1111 1, 1111 2(H+A '), 1111 2(G+B), 1111 24A, 1111 32A, 1111 43(A+B+C) and 1111 47A, where the brightest UV lines (C IV λ1549, Si III] λ1891, C III] λ1909, C II] λ2326, Mg 11 λ2799) were studied, as WC]] as the UV continuum (modeled by a two photon continuum). The quality of the IUE data is rather limited due to the broad point spread function and the low signs.-to-1loisc ratio, and therefore the models

1. Introduction

Herbig-Haro (HH) objects are diffuse emitting regions associated with the supersonic outflow from young stellar objects (YSOs). A large fraction of their UV, optical and near infrared emission is in the form of permitted (e.g Hα, C IV) and forbidden (e.g. [S II], [Fe II]) lines, which arise in the recombination region of the shock excited gas (Schwartz 1975), a consequence of their supersonic interaction with the surrounding medium. The HH condensations in many cases resemble morphologically working surfaces, which are characterized by two shocks, the Mach disk (or jet shock) and the bow shock (e.g. Hartigan 1989; Raga 1989). in detail, however, their structure is more complex, as ground (Eislöffel et al. 1994) and HST images (Hester et al. 1994) have recently revealed.

Several of the intrinsic properties of such HH objects, e.g. intensity line ratios, position-velocity diagrams, velocity dispersion and their optical *spatial intensity distribution* (hereafter SID), have been modelled in a reasonable way by simple kinematical bow shock models. The success on these models relies on the difficulty in spatially resolving for most targets the Mach and bow shocks; that the bow shock allows the simultaneous presence of strong shocks at its apex, and weaker shock at its wings; and finally, that for the typical estimated jet and preshock densities (Raga & Noriega-Crespo 1993)

1 UE data and 'degraded' optical observations has been previously carried out by Lee et al. (1 988), the comparison with the shock models should provide a more clear understanding of the physical conditions in 1111 objects. The IUE data has been collected from the published literature (Lee et al. 1988; Böhm et al. 1987; Böhm et al. 1991; Böh m et al. 1992; Böhm et al. 1993) The objects studied arc 1111 1, 1111 2, HH 24A, HH32, HH 43, and HH 47, with a particular attention to their stronger emission lines: C IV λ1549, C III] λ1909, C II] λ2326, Mg II λ2799, Si III] λ1891 (if available) and the continuum.

A description of the properties and limitations of the kinematical bow shock model is presented in §1, and of the shock models for the selected lines in §3. The characteristics of the individual 11 II objects are discussed in §4, and we present our concluding remarks in §5.

It is shown, as suspected from the optical observations (Eislöffel et al. 1994; Hester et al. 1994) and model position-velocity diagrams (Indebetouw & Noriega-Crespo, 1995) that the match between theory and observations improves when the presence of multiple condensations is considered in their interpretation.

2. The Kinematical Bow Shock Model

2.1. Geometry

A detailed description of a simplified Low shock model can be found for instance in Hartigan, Raymond & Hartmann 1987 (hereafter HRH87). The basic idea is the following. In the frame of reference of the shock, the preshocked gas enters the bow shock at a velocity VS, and angle ξ (see Figure 1). To simplify the calculations of the line emission, tile bow shock is divided into a number of annuli of constant ξ. Once the shape of the bow shock is known (at an orientation ϕ), ξ and therefore the perpendicular component of the velocity, $V_\perp$, can be determined. Since it is only this component which transforms its kinetic energy into internal

energy, the emission from each annulus is calculated running a plane-parallel shock model with velocity equal to its corresponding V_J. This emission, which is considered to be generated in an infinitesimal shell, is then weighted by the area of the annulus and co-added with the emission coming from the rest of the annuli, giving the line emission over

density (100, 1000 cm^{-3}), and (4) the preshock ionization state of the gas. For this last one fully ionized or local equilibrium were the choices (see HRH87), although it is known that the preionization structure in a bow shock is more complex, and that in many comparisons equilibrium models seem to match better the observations (Noriega-Crespo et al. 1989) In all cases, given the wide aperture of IUE, the models considered a slit 10 times the size of

in the fully preionized shock models for the Mg II $\lambda 2800$ line, become amplified by the extent emitting area of the bow shock wings.

2.3. Limitations of the model

e.g. review by Böhm 1990), nevertheless is one of the few instruments that have provided us with simultaneous information of the spatial and spectral properties of these objects at Ultraviolet, wavelengths. The main caveats to study the 1111 objects SID in the UV are due to their relatively low surface brightness, the fact that they are found in star forming regions which arc not necessarily transparent to the UV light, plus the limited spatial resolution given the broad PSF of the IUE telescope.

To deal with these problems, we have concentrated 011 the shape of the *formalized* intensity distribution for a given line, avoiding reddening corrections. We have performed also a convolution of the models with the IUE PSF to avoid deconvolving the observations, which it is proven to be more difficult and less reliable (see e.g. Lee et al 1988). The IUE PSF varies as a function of wavelength, and so it was taken as a Gaussian with a FWHM of 4", for the C IV and Mg II lines and 5" for C]]], C III], Si III] and the continuum (de Boer & Meade, 1 981). Sine.c the size! for many of these objects, from the ground at optical wavelengths, are ~ 5 most of the spatial details are lost in the convolution. If the size of the UV emitting region, however, is *larger* than 5" , then it becomes very interesting the comparison with the models as well as their interpretation (see below).

In the present models the angle between the slit and

same exposure, is identical. We selected C IV λ1549 for the short and C II] λ2326 for the long wavelength ranges to match the maxima.

Since 1111 objects arc not point sources, but diffuse emitting regions with a given morphology, it is necessary to know the orientation of the slit with respect to the object, which depends on the spacecraft roll angle and the orientation of the object in the sky. This information} now is easily available from the IUE data base home page (*http://banzao. gsfc.nasa.gov/IUE/search*). Optical images in [S II] and H-alpha were used to determine the position angle of the objects (see section 3.2 for references). The order numbers in the spectra increases in the direction from the large aperture toward the small aperture for the SWP and LWR cameras, and it goes in the opposite way for the LWP camera (Turnrose et al. 1984).

Finally bear in mind that when comparing models with the IUE observations of HH objects, most of the published data *do not* show error bars. For the brightest objects like 1111 1 and 11112 a typical estimate of the uncertainties in the fluxes is ~ 10%-15Y0. For fainter objects like 1111 43, HH 47 and specially HH24 the uncertainties can be a lot larger.

3.2. The Spatial Intensity Distributions

The physical parameters for the models were obtained from ground base optical studies (a list Of them is S]1OW11 in table 2). The initial parameter space was based 011 the best available shock velocities, proper motions, radial velocities and optical spectra. In some cases the input numbers for the models were

sky with respect to the observer, and the angle between the symmetry axis of the object and the position of the slit. in practice we found that this second angle did not make a significant

photon continuum flux (HRH87). The obser vations have been gat hered from those published by Lee et al. (1988), Böhm et al. (]987), and Böhm et al. (1993).

4. Discussion on Individual Objects

4.1. HH 1

1111 1 is a high-excitation object and one of the brightest in the ultraviolet (together with 1111 2). We have modeled it as a single condensation with a shock velocity of 175 km S--l, an orientation angle ϕ = 5 ° (moving into the plane of the sky), a preshock density of 100 cm^{-3}, and a radius R_0 = 2". Figure 3 shows a compar ison between the IUE observations and the models for 2 selected emission lines: C IV λ1550 and Si 111] λ1891, and two 200 Å wide continuum bands, 1500-1 700 & 1700 1900 Å. These models assume equilibrium pre-ionization. In Figure 3 (and all the rest) the broken line represents the IUE PSF and the solid line the convolution of the model with the PSF.

It is interesting to notice that the IUE observations are in this case wider than the PSF, which suggests that the condensation was resolved (but see below). The single condensation models arc just slightly wider than the PSF, but not as much as the observations. This would seem to indicate that the UV emission is not limited to only

exposure, which was taken at a, similar orientation and roll angles, it dots look broader.

The comparison between model and observation leads to at least two tilings, one that the preonization is not entirely near equilibrium. The full preionized models, although do not look like the observations and overestimate the integrated fluxes, have in general SID with a more extended shape. An intermediate

al. 1991, Böhm et al. 1990).

Observationally (see Figures 4a,b), the distributions for the C IV and C 111] lines in the SWP18157 and SWP40663 frames are wider than the point spread function (broken line). This was the first indication of contribution of more than one condensation to the UV light. The superimposed double bow shock model (1ocs a very good job in matching the extent of the SWP40663 lines (Figure 4a). The 'hump' of the model distribution suggests that the double peak structure that is observed is for real and not an artifact of the 1 UE observations. At a different orientation for the SW]']8157 frame, the superimposed model resembles that observations both in shape and extent.

'1'here is another condensation that has been observed in HH 2: HH2G. The optical images suggest that 1111 2G emission may have a contribution from 1111 2B within the IUE aperture, so once again we tried the superposition of two bow shocks to model

order were considered, The models in Figure 4c correspond to 110 km s^{-1} for HH 2G and 105 km s^{-1} for HH 2B. The observed distributions for C IV and C III] from the SWP43891 set (Böhm et al. 1993) are again broader than the PSF. The superimposed double bow shock model does match well the extent of the C III] line and it is somewhat narrower than the observed C IV distribution, One suspects that a more realistic preionization in the models could give even a. better match.

4.3, HH 24A

HH 24 is optically a remarkable object with a very complex morphology, and situated among two or three outflows (see e.g. Mundt, Ray & Raga 1 991). One of the bright Condensations corresponds to HH 24A which was observed in the UV by Böhm et *al.* (1992). HH 24A although optically seems to be a high excitation object (see e.g. Brugel et al, 1981) in the UV does not belong neither to the high nor to the low excitation categories (Böhm et al. 1992). The lack of UV emission lines has lead to the analysis of just its continuum emission, which it has a SID wider than that in the [S II] 671 7/31 optical lines (Böhm et al. 1992), for instance.

Despite the complexity of HH 24, the extended nature of condensation A, and our temptation to use a superposition of two bow shock models to explain the observed wide SJD, the nearest bright condensation 11]1 24E is $\sim$ 20" apart, and therefore we decide to model it as a single bow shock. We considered two shock velocity models for it. On one hand the proper motions (Jones et al. 1987) and the velocity dispersion of its optical lines, e.g. Hα, [N II] λ6583 and [S II] 6731λ (Solf 1987), suggests a shock velocity relatively low $\sim$ 50 km S-]. On the other hand the detection of [O III] λ5007 (Brugel et al. 1991) implies a shock velocity of $\sim$ 100 km s^{-1}. Both bow shock models (for 50 and 100 km s^{-1}) assume equilibrium preionization with a preshock density of 100 cm^{-3}, a radius of 3 "and an angle of -36° (towards

the observer).

In Figure 5 we show the comparison with the observations of two different 200 Å wide continuum bands, 1300 -- 1500 and 1600 - 1800. The top two panels correspond to the 50 km s- ^{1} model and the bottom one to the 1 00 km S^{-1} model. The comparison with the SWP22708, at an orientation of 153°, with the 50 km s" ^{1} bow shock model looks very good, both observation and model are hardly wider than the PSF. In the next two panels we consider the SW P38033 and SWP38102 observations, taken at slightly different aperture orientation angles $\sim$ 13° apart, but more than 150° with respect the SWP22708 (see Table 1). The observed SI Ds are considerable wider than the calculat ed at 50 km s^{-1} (middle pane]), as was the case with th optical lines (Böhm et al. 1992). The 100 km s^{-1} model (bottom panel) looks Letter thanks to the tail generated by the low velocity shocks, but still it is not as

of the extinction at smaller wavelengths (Lee et al. 1988). We consider bow shock models at two different orientation angles in the plane of the sky, 30° (Davis et al. 1996) and 70° (Self, Böhm & Raga 1 986). Based on the mentioned spectroscopic data and radial velocity measurements, plus 1111 32A proper motions (Herbig & Jones 1983) we selected a shock velocity of 300 km s^{-1}. A preshock density of 100 cm $^{-3}$ and a radius of R_0 = 2.5 "were used. Models at both preionizations were calculated, but in this case the completely ionized models, snow in Figure 6, resemble more the observed S]])s. The LWR1 3004 observations are wider than the PSF (broken line) and with a tail; a trend reproduced by the models at 30° (top) and 70° (bottom).

4.5. 111143 and 1111 47A

Both HH 43 and 1111 47A are low excitation objects, with spectral features from fluorescent H_2 emission and UV continuum (Böhm et al. 1991). Because of the lack of available one-dimensional H_2 emission shock models from HRH87, we have focused on the distribution continuum emission from both objects. In Figures 7 & 8 we show the S11)s for 111143 and HH 47A, respectively, for the SWP24924, LWP4041 , SWP31828 and SWP33960 observations.

The 1111 43 system was modeled as a triple condensation (A+B+C) with a preshock density of 100 cm^{-3} and equilibrium preionization for each condensation. From the analysis of the data presented by Schwartz (1988), 11]1 43A was modeled with a shock velocity of 100 km s^{-1} at an orientation angle of 60° into the sky, For 1111 43]1 the shock velocity was chosen to be 40 km s^{-1} at an angle of

1111 43A/4311 and 43B/43C pairs their distances are 5.5'' /6.9", 6.9"/6.9" and 6.6'' /7.5" for 304°, 1 59° and 146° orientation angles, respectively.

The observed S11)s are wider than the PSF by almost a factor two. The SIDs are so wide that even the 3 condensations models do not match exactly their extent. The models, nevertheless, trace the correct trend of a more extended 'wing' emission from the UV continuum.

5. Conclusions

The goal of this study has been to use a simple kinemati cal model to unders tand the spatial intensity dist ributions obser ved in the UV light by IUE of some HII objects. The SID models overall have shown that many of the parameters that have been obtained by optical means provide a self-c.ollsistellt picture when ar c used to explain the UV emission. The models presented here stress the basic idea that to model the emission of these

It is a pleasure to thank Eileen Friel for her support and helpful comments. A.M-M. was supported by a Perkin Fellowship during her stay at MMO. A.N.-C. research is supported by NASA Long Term Astrophysics Program through JPL under contract with Caltech, and NSF grant AST9300391 through MMO.

REFERENCES

Böhm, 1{,11., Buhrke, 'PlJ., Raga, A. C., Brugel,E.W., Witt, A.N., &Mundt,R. 1987, ApJ, 316, 349

Böhm, K.H. IWO, in "Evolution in Astrophysics, IUE Astromomy in the Era of New Space Missions", ESA Conf. pmt. sp-310, p23

Böhm, K.H., & Solf, J. 1990, ApJ, 348, 297

Böhm, K.H., Scott, D.M ., & Solf, J.

Eislöffel, J., & Mundt, R. 1994, A&A, 284, 530

Hartigan, P., Mundt, R., & Stocke, J. 1986, AJ, 91, 1357

Hartigan, P., Raymond, J., & Hartmann, L. 1987, ApJ, 316, 323

Hartigan, P., 1989,

Solf, J., Böhm 1{.11., & Raga, A.C. 1986, ApJ, 305, 795

Solf, J. 1987, A&A, 184, 322

Turnrose, B.E., & Thompson, R.W. 1984, IUE Processing Manual (Computer Science Corporation, Beltsville, MD).)

This manuscript was prepared with the AAS LaTeX macros v4.0.

Figure Captions

Figure 1. Bow shock geometry. The gas enters the bow shock at a velocity V_S and angle ξ. The parallel component of the velocity ($V_{parallel}$) is conserved across the shock, perpendicular component is thermalized (from $V_{perp}i$ to $V_{perp}f$). The angle between the plane of the sky and the symmetry axis of the bow shock is ϕ.

Figure 2. A sample of the spatial intensity distributions (S1 D) created by the kinematical bow shock model for the high excitation C IV λ1 549 and the low excitation Mg II λ2799 emission lines (top panels). The models correspond to a set of shock velocities of 100, 150, 200, 250 km s^{-1}, at two different initial gas preionizations: equilibrium (eq) and

-- 1800 Å for 1111 24A. The observations correspond at two different aperture orientations. The SWP22708 (top) and SWP38033/1 02 (center) distributions are compared with a model with a shock velocity of 50km s^{-1}. The SWP38033/102 set (bottom) is also compared with a model at a 100 km s^{-1} shock velocity.

Figure 6. As in figure 3, but for the Mg II λ2799 line in IIII 32A. Two models with different viewing angles are compared: 30° (top) and 70° (bottom), with the same 300km s^{-1} shock velocity.

Figure 7. As in Figure 3, but for the 111[43(A+B+C) system and a triple condensation model and three different continuum observations: 200, 400 and 600 Å wide, respectively.

Figure 8. As in Figure 3, but for the 600 Å wide continuum distribution of 1111 47A.

Table 1. Archival IUE Spectral Data

Name object	Image 110,	Exposure time(min)	Orientation angle(deg)	Roll angle(deg)	Year of observation
HH 1	SWP 8188	270	337	95.9	1980
	SWP16668	270	348	84.6	1982
	SWP24914	729	303	130.5	1985
	SWP40657	633	315	124.7	1991
	LWR 8912	134	167	266.1	1980
1111 2(H-|A')	SWP10218	270	165	268.4	1980
	SWP10246	290	167	266.3	1980
	SWP16671	430	349	84.0	1982
	SWP18157	430	167	266.1	1982
	SWP24919	860	304	129.4	1985
	SWP40663	675	312	123.8	1991
	LWR 8888	180	165	268.4	1980
	LWR 8909	150	167	266.4	1980
	IJWR1045O	380	5	67.8	1981
1111 2G	SWP43891	636	315	119.0	1992
HH 24A	SWP21518	560	189	243.9	1983
	SWP22708	485	153	81.3	1984
	SWP38033	680	307	126.3	1990
	SW1`38102	585	320	113.3	1990
	LWP 3140	120	153	81.3	1984
HH 32A	LWR13004	414	155	-- 99.0	1982
111143	SWP17522	390	132	3 0 1 . 1	1982
	SWP23749	425	147	285.7	1984

Table 1- Continued

Name object	Image no.	Exposure time(min)	Orientation angle(deg)	Roll angle(deg)	Year of observation
	SWP24924	580	304	128.7	1985
	SWP31828	781	159	275.3	1987
	LWP 4041	4?.0	146	286.8	1984
1111 47A	SWP17549	400			

Table 2. Best Fit Bow Shock Model Parameters[1]

Object	V_{sh} (km S^{-1})	4"(°)	Radius(")
HH 1	17{i	5	2.0
HH 2A '	170	12	1.7[2]
			1.83
			2.8[4]
1111211	125	2	2.5[2]
			2.4[3]
			1.54
HH 2G	110	- 5	0.9
HH 2B	105	2	0.4
HH 24A	50	--36	3.0
	100	--36	3.0
1111 43A	100	60	2.3
HH 43B	40	55	2.5
HH 32A	300	30	2.5[5]
	300	70	2.5[5]
HH 43C	35	75	1.8
HH 47A	100	23	3.2

[1]Most models are in equilibrium preionization

[2]Orientation angle 5°

[3]Orientation angle : 165", 349°

[4]Orientation angle 304", 312°

[5]Fully preionized

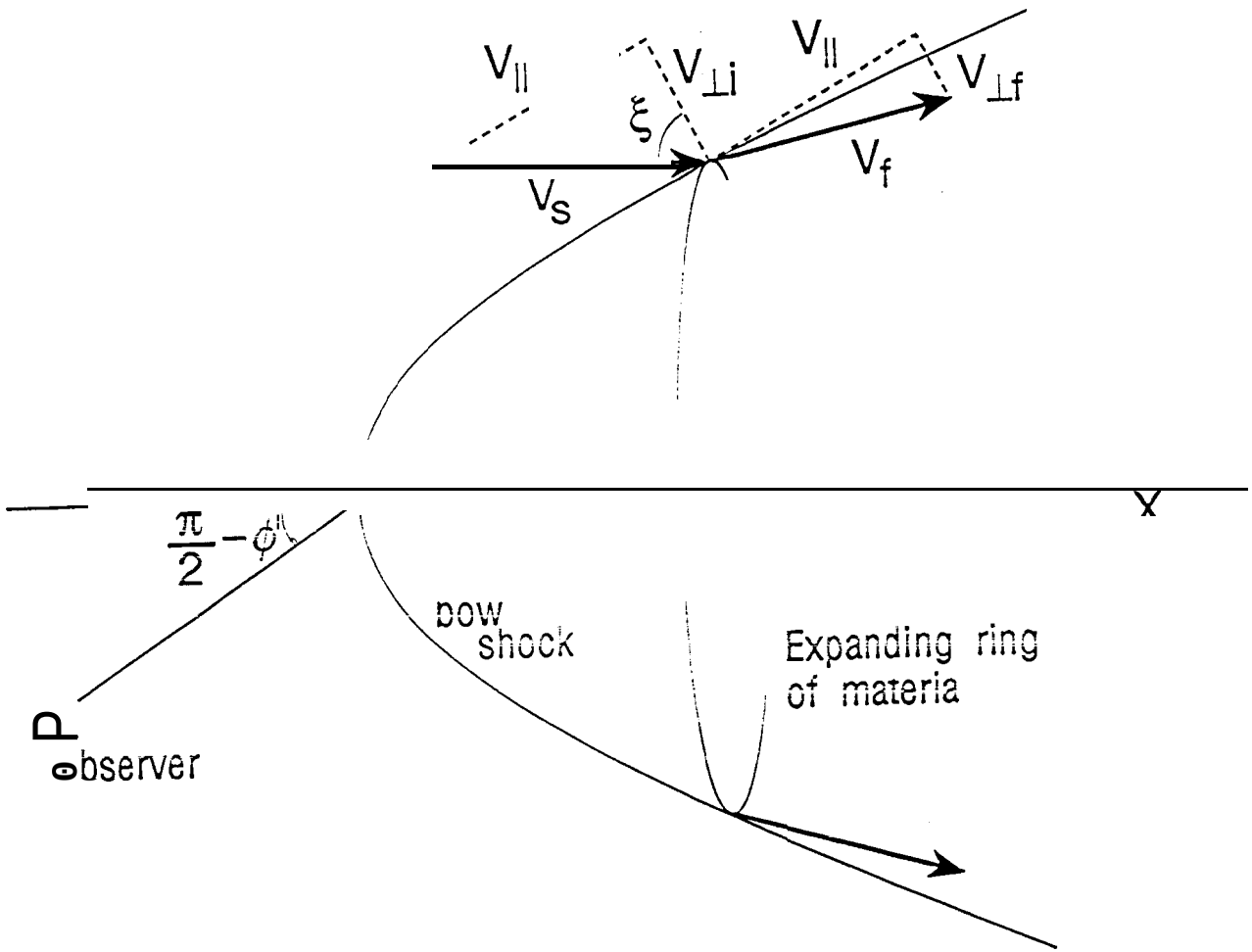

Fig 1
Moro-Martin et al. 19

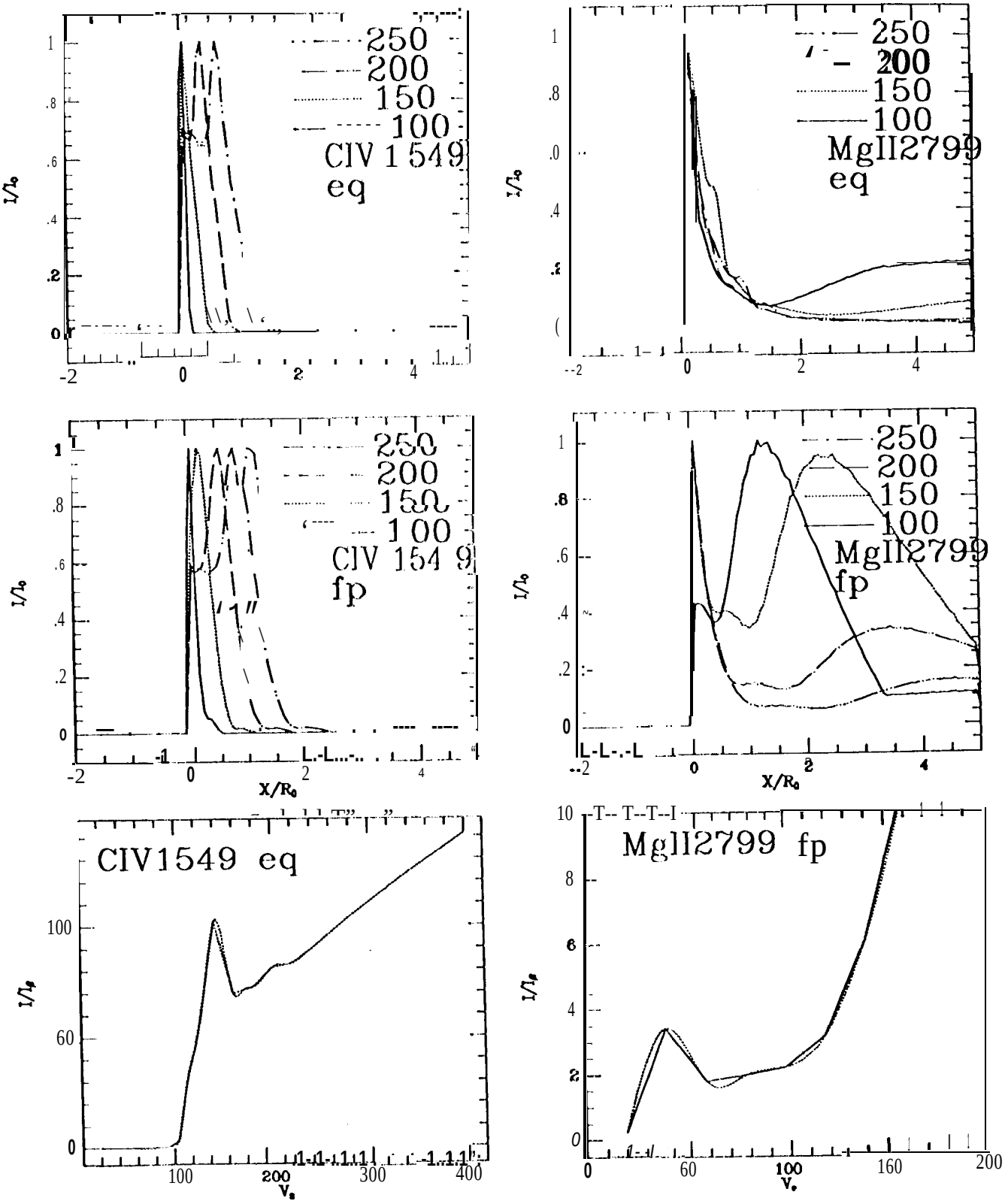

Fig 2.

Moro-Martin et al. 19

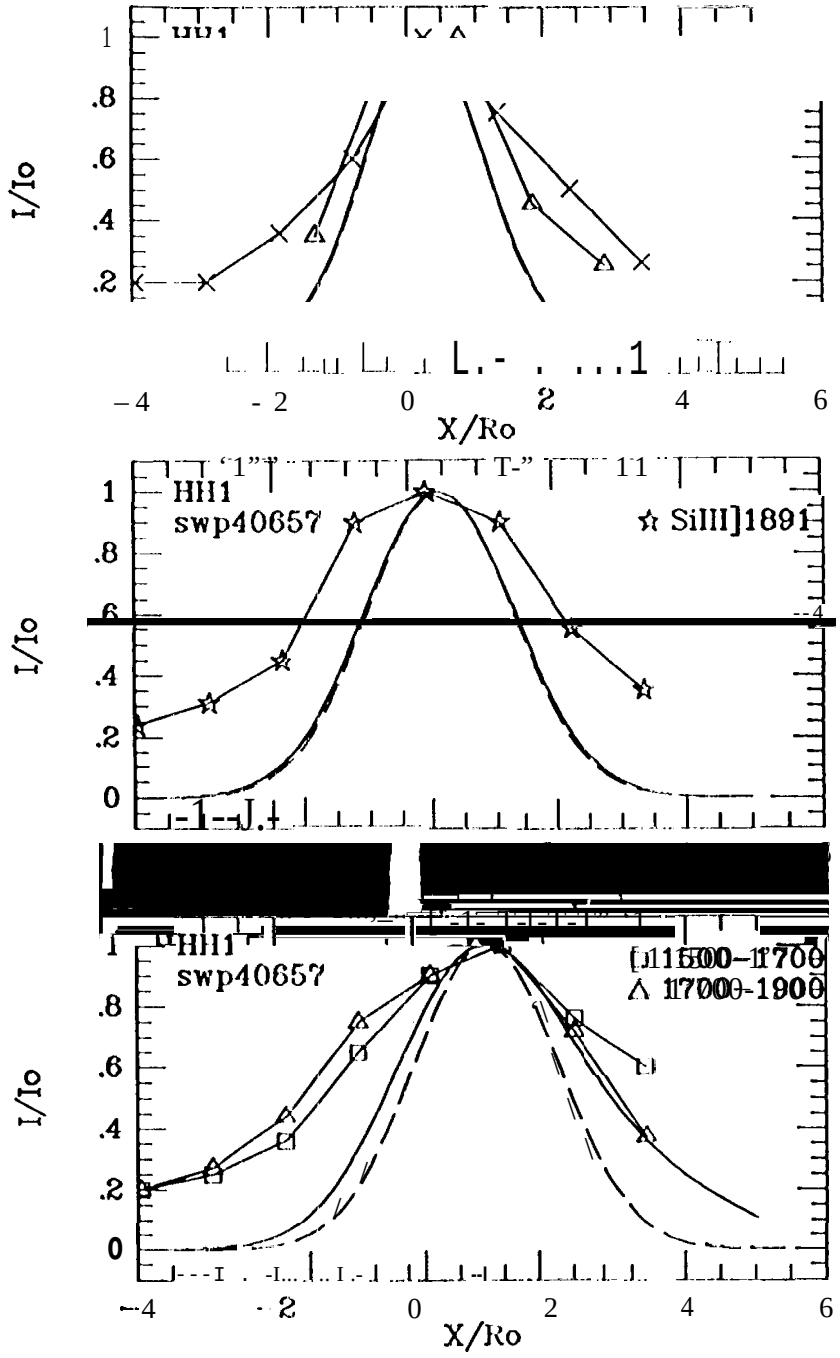

Fig 3.

Moro-Martin et al. 1998

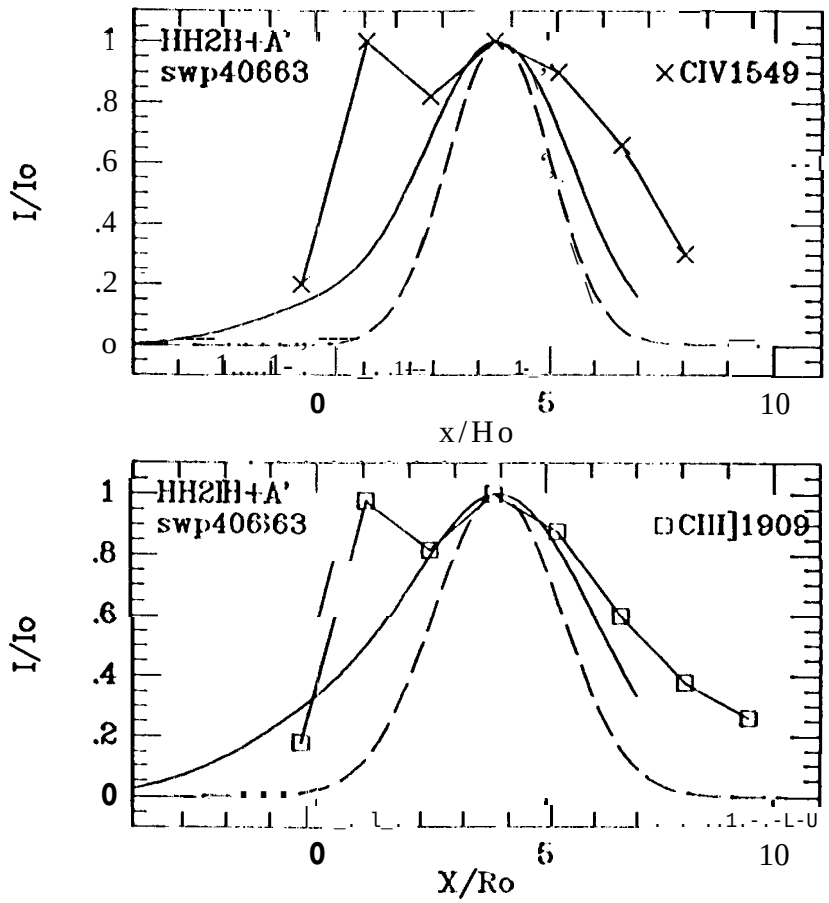

Figure 4a

Moos-Martin et al. 1996

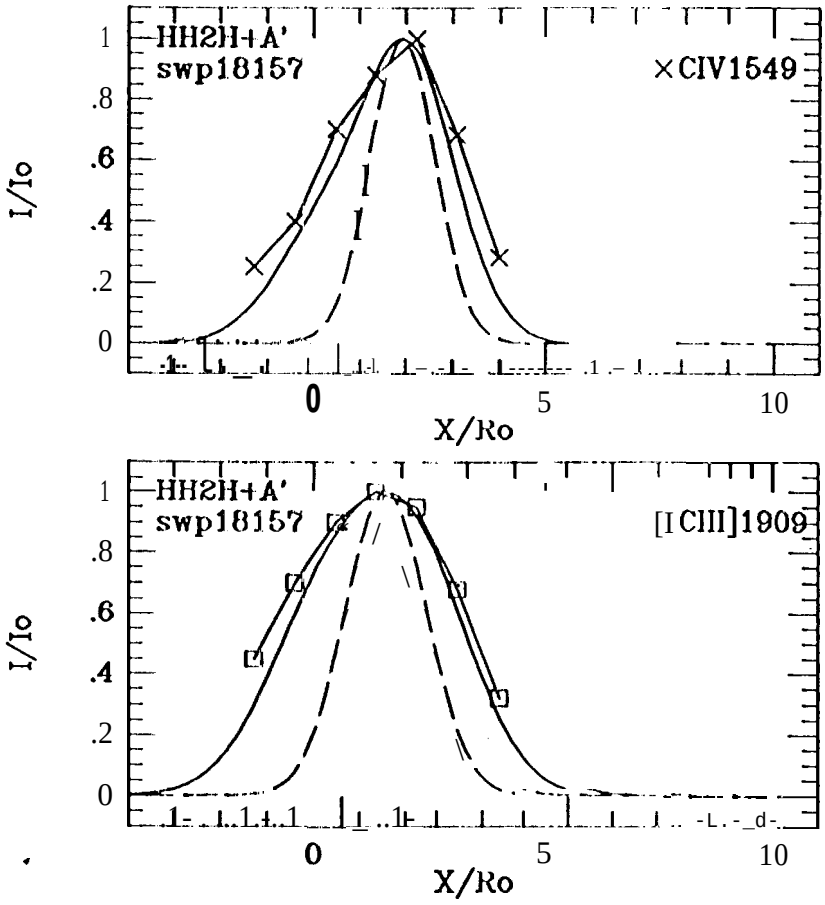

Figure 4b
Moro-Martin et al. 1996

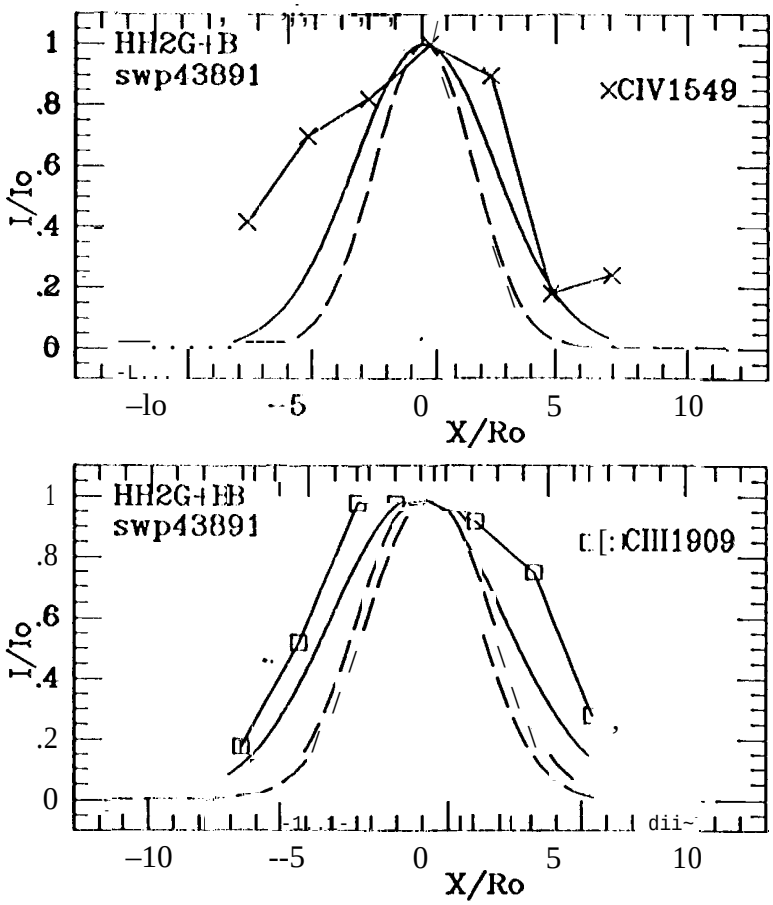

Figure 4c
Moos-Martin et al.

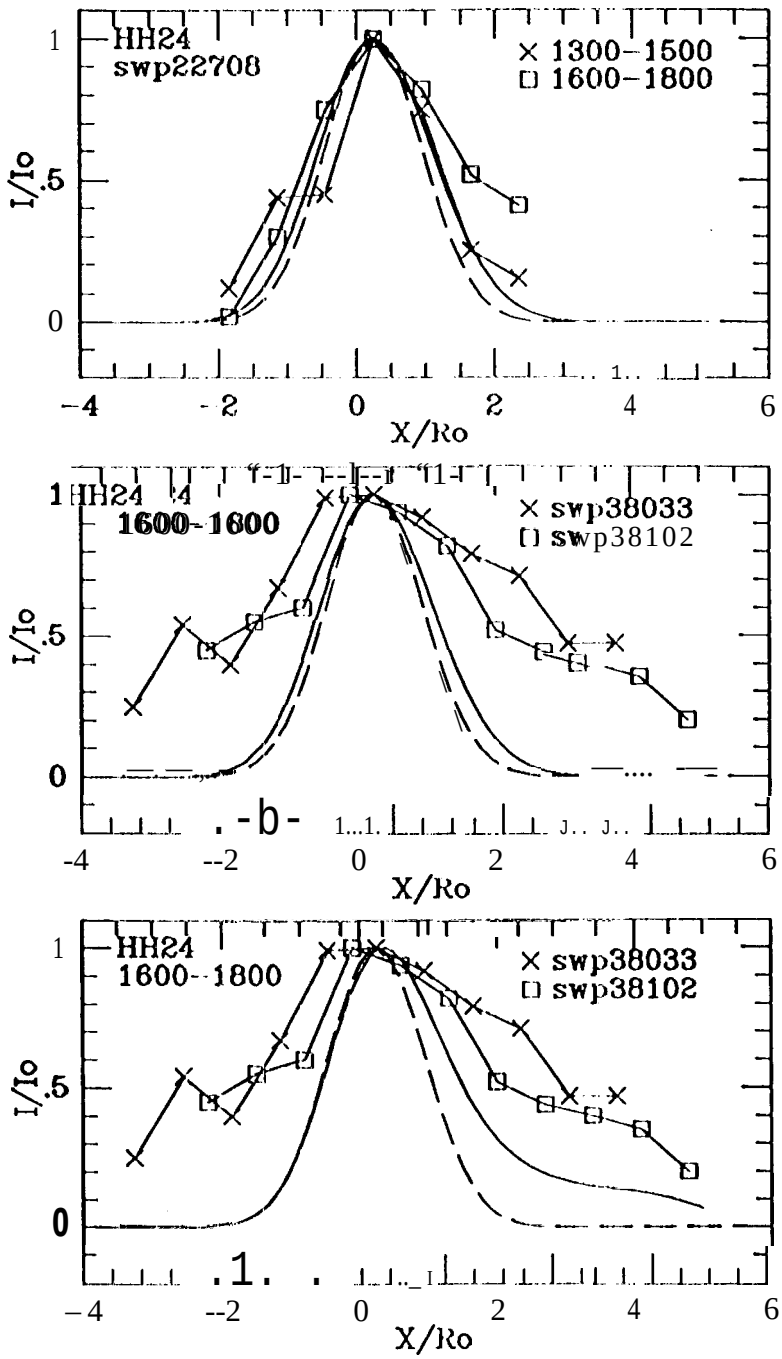

Figure 5
Moo-Martin et al. 1996

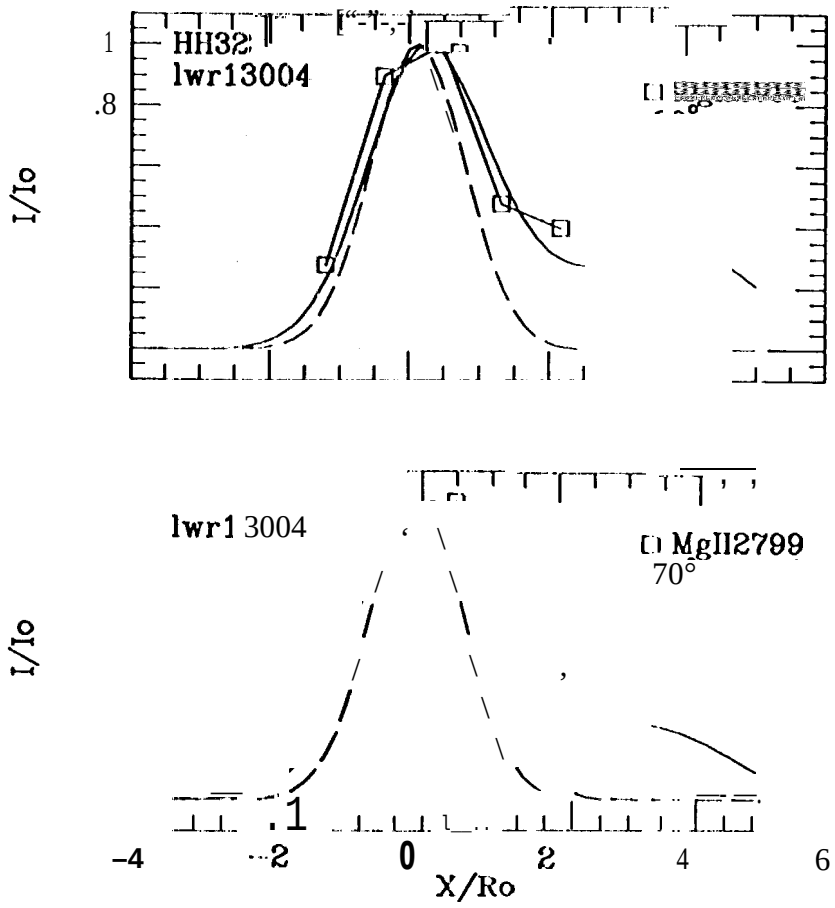

Figure 6

Moro-Martin et al. 1996

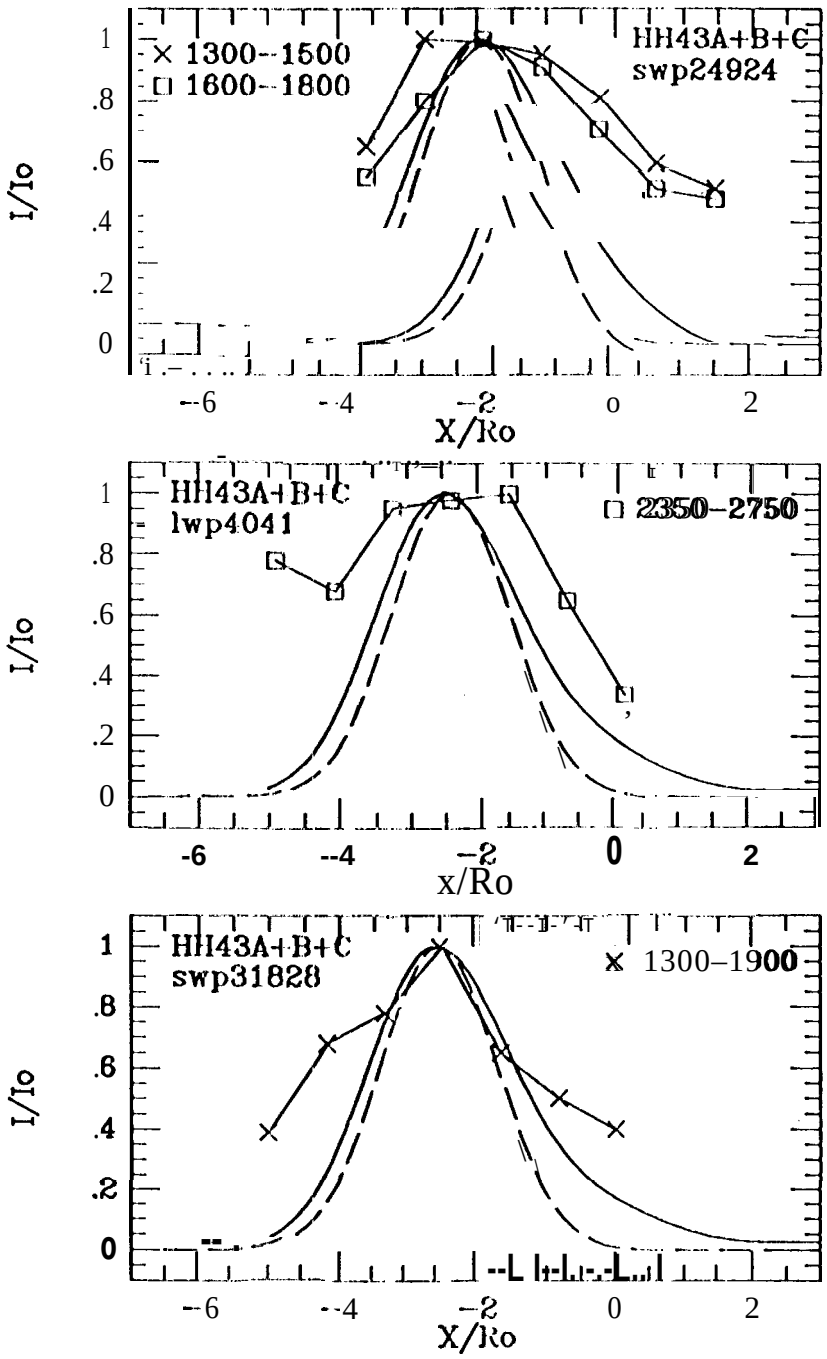

Figure 7
Moro-Martin et al, 19

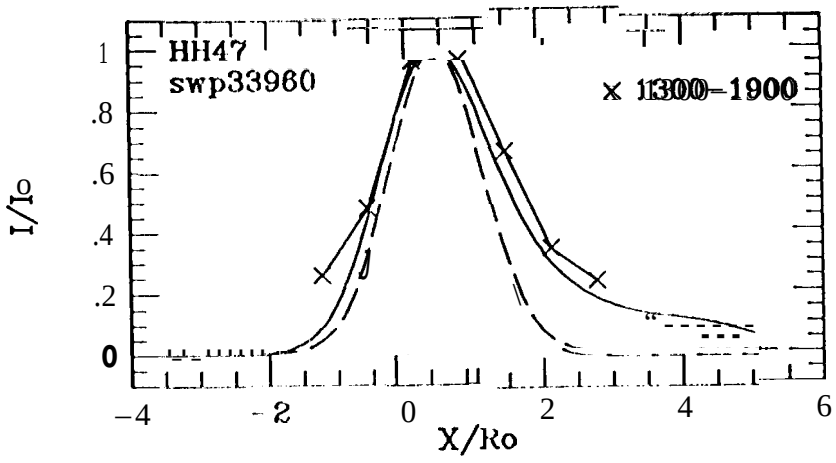

Figure 8
Moro-Martin et al.